Optically Controlled Thermophoretic Trapping of Single Nano-Objects

Marco Braun and Frank Cichos*

Molecular Nanophotonics Group, Institute of Experimental Physics I, Universität Leipzig, 04103 Leipzig, Germany

ABSTRACT Brownian motion is driven by thermal fluctuations and becoming more efficient for decreasing size and elevated temperatures. Here, we show that despite the increased fluctuations local temperature fields can be used to localize and control single nano-objects in solution. By creating strong local temperature gradients in a liquid using optically heated gold nanostructures, we are able to trap single colloidal particles. The trapping is thermophoretic in nature, and thus no restoring body force is involved. The simplicity of the setup allows for an easy integration and scalability to large arrays of traps.

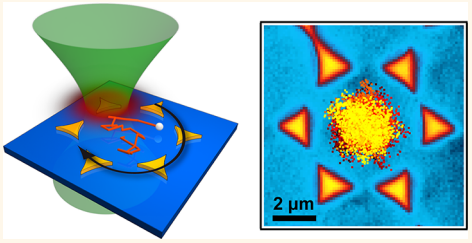

KEYWORDS: plasmonics · thermophoresis · Brownian motion · trapping · nanofluidics

Manipulating the motion of single nano-objects in solution has become an important demand in modern soft-matter sciences, *e.g.*, to study their long-time behavior without mechanical immobilization. The most successful tool is the optical tweezer,[1] which has been developed into a powerful technique in biological sciences over the years.[2,3] However, optical tweezing is limited to the manipulation of mesoscopic systems. Such limitations led to the development of multiple new approaches to manipulate the motion of nano-objects. Within the past decade, techniques such as plasmon-based nano-optical tweezers[4,5] and the anti-Brownian electrokinetic trap (ABEL)[6] have been proposed. The ABEL trap is capable of localizing even single molecules utilizing electric fields and an optical feedback.[7,8] More recently a new variant of the Paul trap has been demonstrated to work in liquids confining small objects to a tiny volume.[9] Both the ABEL and the Paul trap use rigid metal nanostructures to generate electric fields introducing topographic constraints for wiring and contacts to the system. Hence, an extension of the techniques for a free manipulation of particles in solution that goes beyond trapping is not easily possible.

Here, we present a method that employs highly localized temperature fields generated by plasmonic nanostructures to confine and manipulate individual nano-objects in solution. While it is counterintuitive that elevated temperatures, which increase the strength of Brownian fluctuations, should help to eliminate Brownian motion, we show that the well-known Ludwig–Soret effect[10] provides an efficient mechanism to trap and steer single nano-objects. Thermophoretic trapping of small molecules exhibiting a small Soret coefficient, such as DNA or RNA and colloids involving temperature gradients and heat-induced convection flows, has been demonstrated before,[11–18] but was limited to large ensembles of molecules and colloids only. This report extends the thermophoretic trapping to single nano-objects in solution and exemplifies the manipulation of these objects in a single trap. The required metal nanostructures are prepared by microsphere lithography (see Materials and Methods section) and provide scalability to large arrays of traps, which could then lead to a controlled assembly of single nano-objects in solution and a multitude of new studies focusing on the interactions of even single molecules.

The Ludwig–Soret effect is based on a temperature gradient along the surface of a nano-object that leads to an interfacial fluid flow, which in turn moves the nano-object through the solution without a body force acting.[19] The resulting drift velocity of the nano-object, $\mathbf{v}_T = -D_T \nabla T$, is proportional to the temperature gradient, ∇T, and the thermodiffusion coefficient, D_T, which yields the mobility of the particle in the temperature

* Address correspondence to cichos@physik.uni-leipzig.de.

Received for review September 24, 2013 and accepted November 11, 2013.

Published online November 11, 2013
10.1021/nn404980k

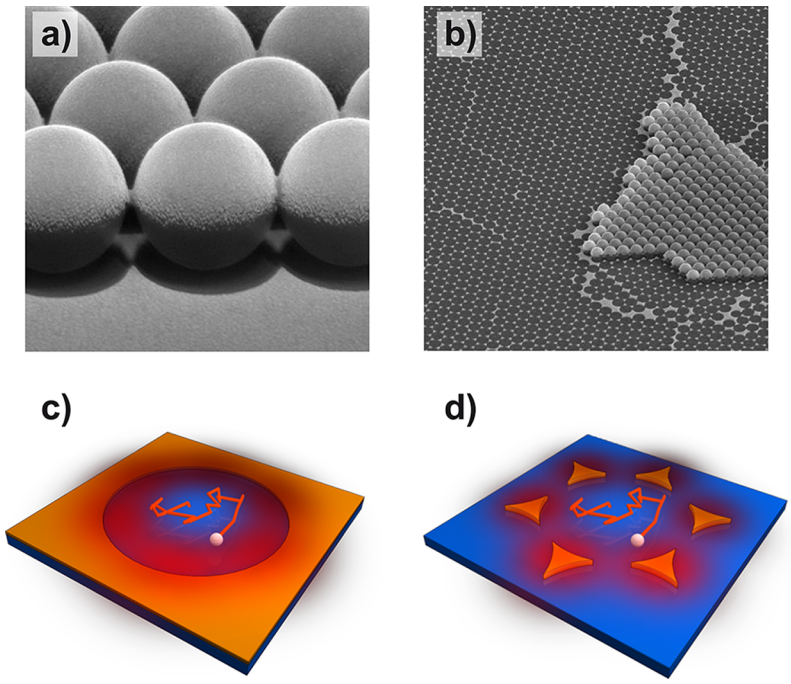

Figure 1. (a) Scanning electron microscopy (SEM) micrograph of a 50 nm gold film on top of 5 μm polystyrene (PS) beads and a cover-slide. (b) SEM micrograph of a hexagonal microarray of single gold islands. (c) Sketch of a closed gold structure sample consisting of a 5 μm diameter hole in a gold film. (d) Same as in (c) for an open gold structure sample that is composed of triangular gold pads (edge length about 1.5 μm) in a hexagonal lattice on a glass substrate.

gradient and comprises a number of different contributions to thermophoresis.[20,21] Typically, one of the strongest contributions comes from a temperature-induced distortion of the counterion cloud around the nano-object, which causes the object to move from the hot to the cold. The so-called Soret coefficient compares the thermodiffusivity to the isothermal diffusivity, $S_T = D_T/D$. As the thermodiffusion coefficient, the Soret coefficient S_T is positive for a motion against and negative for a motion along the direction of the temperature gradient. The Soret coefficient is typically on the order of $S_T \approx 0.01 - 10\ K^{-1}$ depending on the object size and a variety of other properties, *e.g.*, the salinity of the solution and the temperature.[20−22] Hence, diffusion and thermodiffusion are of comparable strength and, thus, well suited to manipulate colloids or molecules in solution.

Within this report we employ plasmonic gold nanostructures as optically controlled heat sources. The plasmon resonance of the metal structures thereby allows an efficient conversion of optical energy into heat. Accordingly, localized temperature gradients of a few 10 K per micrometer are easily generated. An appropriate arrangement of these plasmonic heat sources then provides an optically controlled thermophoretic drift velocity field, allowing for the confinement and manipulation of single nano-objects.

To demonstrate the capabilities of plasmonic structures for heat-controlled nanomanipulation, we have chosen two different gold microstructures. These structures resemble a circular hole in a thin gold film of 50 nm thickness on a substrate and a periodical structure consisting of single gold pads in a hexagonal array as obtained from colloidal sphere lithography (Figure 1; see Materials and Methods for details). Both gold structures can be heated with either an expanded or a focused laser beam. The expanded laser beam allows for a continuous heating of the entire gold structure, while the focused laser provides a local heating, which can be dynamically changed.

The heat generated in the gold structure is released to the liquid and the glass substrate in the local environment. Since the sample represents a large heat bath at ambient temperature T_0 as compared to the small structures, a steady-state temperature profile, $\Delta T(\mathbf{r})$, appears in the liquid above the gold structure. We have calculated the corresponding temperature profiles for a specific trap diameter by finite element simulations directly at the gold structure as well as 300 nm above it (see the Supporting Information (SI) for details). The relative temperature profiles depicted in Figure 2 are completely defined by the temperature rise at either the gold surface, ΔT_{Au}, or the trap center, ΔT_{center}. The main difference of the two structures is in their depth, $\Delta T_{Au} - \Delta T_{center}$. For example, the temperature rise in the center of the hole structure is about 83% of ΔT_{Au}, while it is only about 37% for the patchy structure. Thus, considerably lower temperatures can be achieved in the trapping region, which might be of advantage for the trapping of temperature sensitive objects such as DNA or other biologically relevant objects. Further, larger temperature gradients result

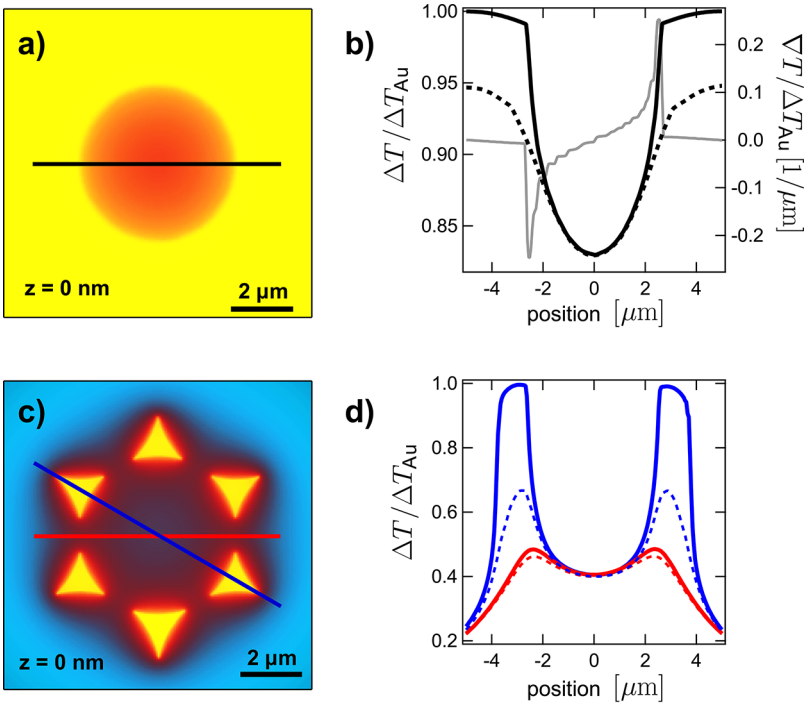

Figure 2. Simulated temperature profiles (a) within the closed gold structure sample laterally through the gold structure. (b) Lateral line profiles along the temperature field (black) and the corresponding temperature gradients (gray) through and 300 nm above the gold structure (dashed). The temperature was normalized to the temperature increase of the gold structure, ΔT_{Au}. Analogous plots for the open gold structure in (c) and (d).

from the localized heat patches (Figure 2c blue line). However, this is only valid for the temperature profiles along a direction connecting two gold pads. Within the gaps between the gold patches along the circumference, the temperature is only 8% higher than in the trap center (Figure 2c, red line). For both gold structures, the center temperature rise, ΔT_{center}, decreases with increasing trap diameter, as shown in the Supporting Information. Considering only the central region of the temperature profile reveals a parabolic shape (eq 1).

$$\Delta T_{harm}(r) = \frac{\alpha}{2} r^2 + \Delta T_{center} \quad (1)$$

This parabolic temperature profile is defined by the curvature α, which defines the stiffness of the trap, and ΔT_{center}, which refers to the temperature increment at the center of the structure as compared to the ambient temperature, T_0.

RESULTS AND DISCUSSION

Trapping of Single Polystyrene Spheres in a Closed Gold Structure. The confinement of a single 200 nm polystyrene (PS) nanoparticle in the closed gold structure heated with an expanded laser is readily observed from the single-particle positional distribution in Figure 3a. At low heating power P_{heat} the particle positions are distributed over the whole circular region. By raising the heating power the particle is increasingly confined to the center of the trap. The spatial distribution of trajectory points is well represented by a Gaussian distribution, and the radial distribution therefore follows a Rayleigh distribution (Figure 3b). The width of this radial distribution function shrinks with increasing heating power, as displayed in Figure 3c, with the particle being confined to an area with $1-2\,\mu$m radius.

The steady-state position distribution can be understood from the balance of thermodiffusion pushing the particle inward and diffusion spreading the particle positions in space.[23] The sum of both probability density current densities, $j_D = -D\nabla p_s(\mathbf{r})$ and $j_{TD} = -p_s(\mathbf{r})D_T(\mathbf{r})\nabla T(\mathbf{r})$, is then zero and yields an exponential probability density distribution $p_s(\mathbf{r})$ for finding the particle at a certain position $\mathbf{r}$ assuming a constant thermodiffusion coefficient D_T (eq 2).

$$p_s(\mathbf{r}) = p_0 \exp(-S_T \Delta T(\mathbf{r})) \quad (2)$$

Inserting the parabolic temperature profile of eq 1 readily unveils a Rayleigh distribution for the radial distribution (see SI).

$$p_s^{rad}(r) = S_T \alpha r \exp\left(-\frac{S_T \alpha}{2} r^2\right) \quad (3)$$

The width σ of the position distribution is given by $\sigma = 1/(S_T\alpha)^{1/2}$. Therefore, the Soret coefficient and the curvature α of the temperature field define the strength of the confinement. In general the Soret coefficient depends on the system and in particular on the interaction of the nano-object with the surrounding liquid.[20,21] While it also may depend on the temperature, we assume that this variation is small

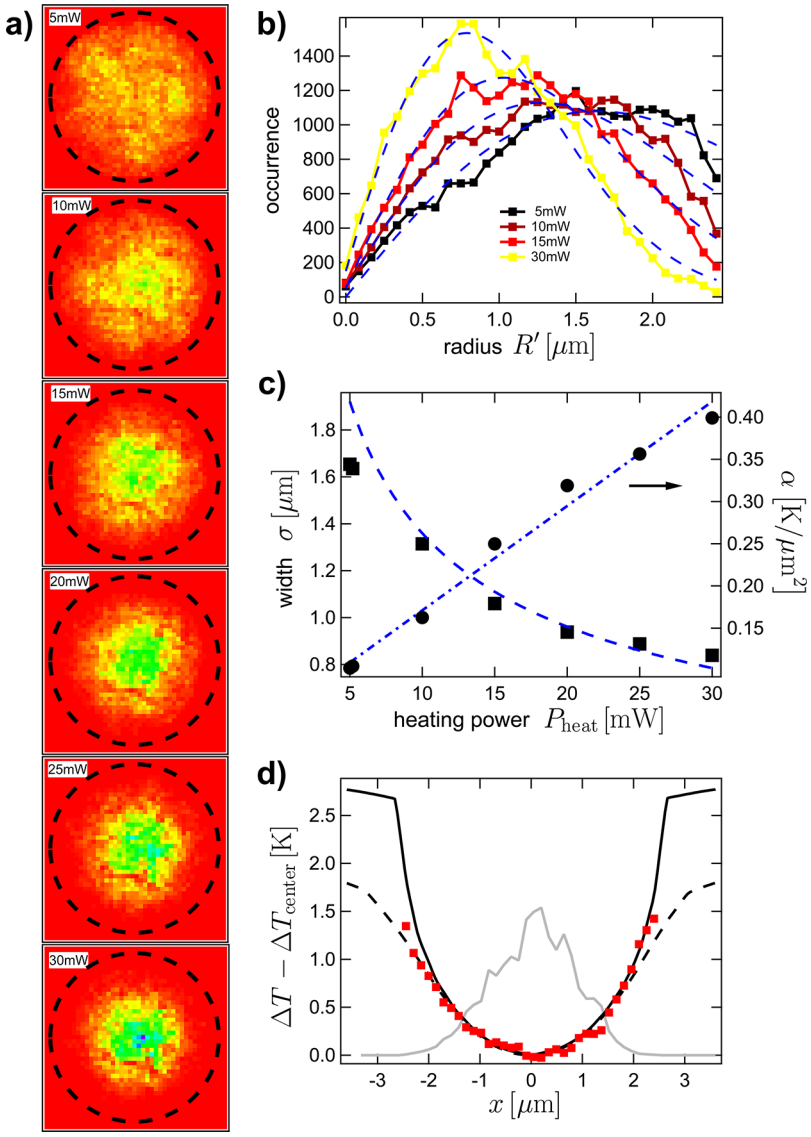

Figure 3. (a) Heating power dependent position distribution histograms of a trapped 200 nm PS sphere. (b) Corresponding radial position distribution fitted with eq 3. R' represents the distance to the center of the trap (see also Figure 4b). (c) Width (σ) of the positions distribution (squares). The fit corresponds to the theoretical dependence of $\propto P_{heat}^{-1/2}$. Curvature of the temperature field α (circles) with linear fit. (d) Temperature distribution (red squares) calculated from the position distribution of the particle within the trap (30 mW, gray and in arbitrary units) compared to the simulated temperature field as in Figure 2b with a temperature offset in the center of the trap of ΔT_{center} = 13.7 K and a Soret coefficient of S_T = 3.56 K^{-1}.

within the given temperature range. The confinement of the particle distribution is therefore controlled by the curvature α, which thus is the relevant parameter for the stiffness of the trap. The curvature α varies linearly with the temperature rise at the gold structure, ΔT_{Au}, which on the other hand depends on the absorbed laser power, $\alpha \propto \Delta T_{Au} \propto P_{heat}$. Consequently, the confinement should depend on the inverse square root of the heating power, $P_{heat}^{-1/2}$ (see SI). This dependence is well reflected in our measurement data in Figure 3c. It implies that nano-objects with different Soret coefficients show the same spatial confinement if the heating power is scaled according to $S_T P_{heat}$ = const.

The similarity of eq 3 to a Boltzmann distribution has been recognized and analyzed before.[15] Here, we just infer that this similarity allows a comparison with other trapping methods. This comparison yields an equivalent potential energy, $\Delta U(\mathbf{r})$, that would be required to confine the particle with a body force, *e.g.*, the gradient force of an optical tweezer. Its ratio with the thermal energy $k_B T_0$ is given by eq 4.

$$\frac{\Delta U(\mathbf{r})}{k_B T_0} = S_T \Delta T(\mathbf{r}) \qquad (4)$$

The depth of this potential ΔU scales with the temperature difference between gold and the center of the trap. It changes linearly with the heating power as well

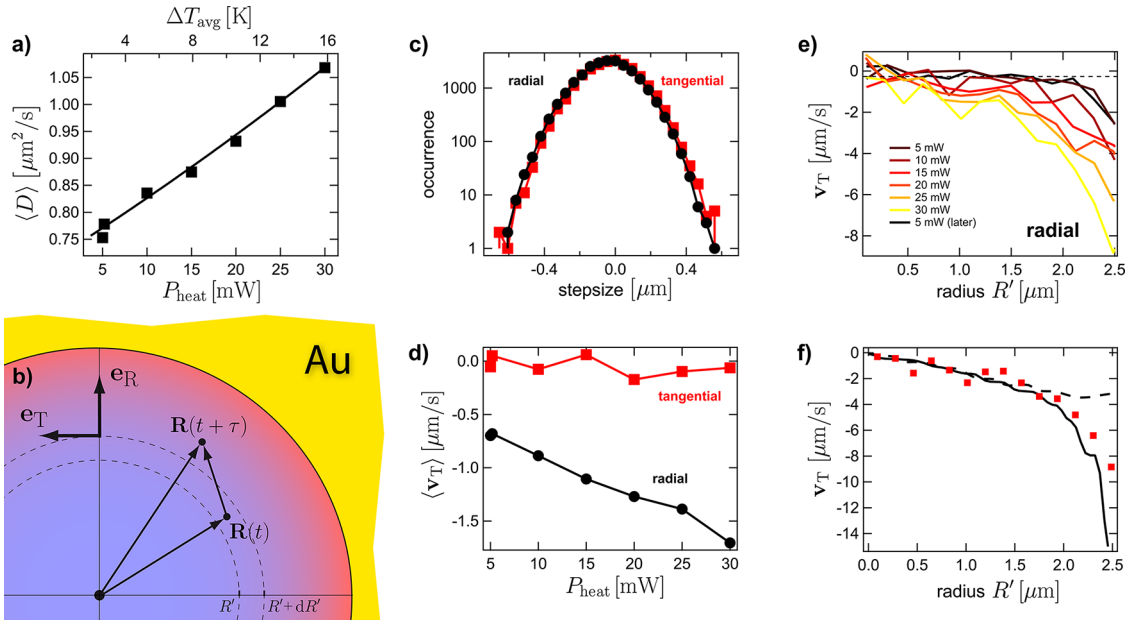

Figure 4. (a) Heating power dependent mean diffusion coefficient of the 200 nm PS particle within the trap. A relation between laser heating power and average temperature rise within the trap was found by fitting the measured diffusion coefficients assuming a Stokes−Einstein relation with a VFTH temperature dependence for the medium's viscosity (black curve). (b) In the stepsize analysis each step $\mathbf{R}(t+\tau) - \mathbf{R}(t)$ of the particle is projected in radial ($\mathbf{e}_R$) and tangential ($\mathbf{e}_T$) directions, where $\mathbf{R}(t+\tau)$ and $\mathbf{R}(t)$ are the positions of the particle in two sequencing frames with a frame time $\tau = 0.01$ s. (c) Histogram of step sizes in radial (black) and tangential (red) directions for the 30 mW heating power trajectory. (d) Average thermophoretic drift velocity within the trap for increasing power of the wide-field laser beam again in radial (black) and tangential (red) directions. (e) Dependence of the radial thermophoretic drift on the distance to the center of the trap and heating power. (f) Comparison between the measured radial thermophoretic drift velocity (30 mW heating power, red squares) and the drift expected from the simulated temperature field in the plane of the gold structure (black) and 300 nm above (black dashed) with a Soret coefficient of $S_T = 3.56$ K^{-1}.

and is also directly proportional to the Soret coefficient. The linear power dependence is equivalent to the power dependence of an optical tweezer for example. However, as the Soret coefficient scales linearly with the radius for colloidal particles,[22] thermophoretic trapping may turn out to be useful for very small particles as well. Inserting typical values of $\Delta T_{Au} - \Delta T_{center} = 10$ K for a Soret coefficient of $S_T = 1$ K^{-1}, we obtain an equivalent trapping potential of $10 k_B T$. Besides the depth of this equivalent potential, we may also obtain a trapping stiffness k. Using a harmonic potential $\Delta U = kr^2/2$ yields $k = \alpha S_T k_B T_0$, which is on the order of fN/m and thus much lower than the typical stiffness of an optical tweezer.[24]

Equation 2 may also be used to determine the temperature profile in the trap, as shown in Figure 3d. This requires prior knowledge of the minimum temperature increment, ΔT_{center}, in the center of the trap and the Soret coefficient, S_T. Both parameters can be determined studying the particle dynamics, *i.e.*, the diffusion coefficient D and the drift velocity $\mathbf{v}_T$. The drift velocity and diffusion coefficient determine the step size distribution of the particle in the trap. This step size distribution is the probability density distribution, $p_d(\mathbf{R}(t+\tau),\mathbf{R}(t))$, of finding a particle at time $t+\tau$ at a position $\mathbf{R}(t+\tau)$ if it has been at position $\mathbf{R}(t)$ at time t. It is described by the advection-diffusion propagator[25] exhibiting a Gaussian shape (eq 5).

$$p_d(\mathbf{R}(t+\tau), \mathbf{R}(t)) \propto \exp\left(\frac{-|\mathbf{R}(t+\tau) - \mathbf{R}(t) + \mathbf{v}_T\tau|^2}{4D\tau} \right) \quad (5)$$

The width of this Gaussian distribution is purely determined by the diffusion coefficient D, while its center is shifted according to the direction and the magnitude of the velocity $\mathbf{v}_T$. Equation 5 is valid only for short time lags τ or small displacements over which $\mathbf{v}_T$ can be assumed to be approximately constant. For an inverse frame rate $\tau = (100\ \text{Hz})^{-1}$ drift velocities of about $\mathbf{v}_T = 5\ \mu$m/s lead to displacements of about 50 nm, which is sufficiently small to carry out the above analysis. Figure 3b displays an example radial and tangential distribution. Analyzing these distributions we find that the diffusion coefficient increases with the heating power from 0.75 μm^2/s at $P_{heat} = 5$ mW to 1.08 μm^2/s at $P_{heat} = 30$ mW. Since this heating power dependence is due to the increased temperature in the trap, we can extract an average temperature rise of $\Delta T_{avg}/P_{heat} = 0.53$ K/mW by assuming a Stokes−Einstein relation with a Vogel Fulcher (VFTH) temperature dependence for the mediums viscosity[26] (see SI). The temperature is averaged according to the distribution of particle positions. Since the particle is located mostly in the center, the average temperature, ΔT_{avg}, differs from the local

temperature minimum, ΔT_{center}, only by about 1.1%. We can therefore assume that $\Delta T_{center} \approx \Delta T_{avg}$. Considering an average temperature rise of 16 K at a heating power of 30 mW, we estimate the temperature increase at the surface of the gold structure to be about 19 K. The confinement is therefore achieved with a temperature difference of about 3 K at the highest used heating power, as seen from Figure 3d.

The key ingredient for the trapping of the particle is the thermophoretic drift velocity induced by the temperature gradient. The drift velocity field can be extracted from the displacement of the center of the Gaussian distribution as shown in Figure 4b. To do so, we employ the trap symmetry and project the displacements to the radial ($\mathbf{e}_R$) and tangential ($\mathbf{e}_T$) direction (Figure 4c). Calculating the velocity components using the inverse frame rate τ unveils a zero tangential and a negative radial drift velocity (see Figure 4d). This negative radial velocity pushes the particle toward the center of the trap. Its magnitude increases linearly with the incident heating power as the temperature gradient is linearly increasing with the heating power. For the highest heating power of 30 mW an average thermophoretic drift velocity of 1.7 μm/s is found, which again represents an average over the spatial distribution of the particle in the trap. The negative velocity is a consequence of a positive Soret or thermodiffusion coefficient. In this case the thermophoretic drift velocity field is convergent with a sink in the center of the trap. In the case of a negative Soret coefficient, the drift velocity field would have a source in the center of the trap, which yields only a metastable trapping.

More detailed information on the radial dependence of the drift velocity in the trap can be obtained by restricting eq 5 to starting points at a certain distance range $R' < R(t) < R' + dR'$ from the trap center. Figure 4e depicts the radial component of the thermophoretic velocity as a function of the distance R' from the trapping center for increasing heating power. The drift velocity is strongest in the outer regions of the trap near the gold structure. Here, the temperature gradient is strongest and radial velocities up to 8 μm/s are measured. Toward the center the temperature gradient and the radial thermophoretic drift disappear almost linearly as the gradient varies linearly due to the parabolic temperature profile. The tangential drift velocity is zero within errors at all distances from the trapping center and at all heating powers.

The radial dependence of the drift velocity can be compared to the predictions based on the temperature profile and the Soret coefficient. The local temperature is completely determined by the simulated relative temperature profile of Figure 2b and the value of the center temperature, ΔT_{center}, which is well approximated by the average temperature, ΔT_{avg}. The Soret coefficient can then be determined by choosing a value for which experimental and predicted radial drift velocity profiles match ($\mathbf{v}_T(r) = -D_T\nabla T = -S_T D\nabla T(r)$). This comparison yields a best match for a Soret coefficient of $S_T = 3.56\ K^{-1}$ (see Figure 4f). This Soret coefficient is about a factor of 3 larger as compared to the results of Braibanti *et al.*[22] This increase can be attributed to the confinement of the particles by the two glass slides in the *z*-direction. The hydrodynamic interaction with the glass surface increases the effective friction.[27] For the free diffusion of the particles we find that the diffusion coefficient is decreased by a factor of 3 as compared to the expected Stokes–Einstein value. The corresponding thermodiffusion coefficient D_T, however, remains unchanged since the involved interfacial flows are much more short ranged.[28] As the Soret coefficient is the ratio of thermodiffusion and diffusion coefficient, the decreased diffusion coefficient leads to an increased Soret coefficient. Considering again the effective potential that corresponds to the positional distribution of the particles in the hole trap, we find a potential depth of 10.7 k_BT for an incident power of P_{heat} = 30 mW under wide-field illuminaton.

Trapping of Single Polystyrene Spheres in an Open Gold Structure. Trapping can be achieved not only in a closed gold structure as presented above. An open patchy gold structure as displayed in Figure 2d may be used as well. The major difference of this structure from the closed one is that the temperature field is localized at the patches. This further increases the local temperature gradient and decreases the average temperature in the trap. For the study of particle motion in this periodical gold structure sample, we introduce a dynamic heating with a focused laser. The laser spot is steered to move along a circle with a diameter that matches the gold structure as sketched in Figure 5a. The rotation frequency is set to 19 Hz, which corresponds to a velocity of the temperature field of about 315 μm/s and thus is much faster than the thermophoretic drift velocity. Hence, the particle feels a steady-state temperature profile. Figure 5b displays the trajectory of a single 200 nm PS sphere in an open trap geometry and directly proves that single particles can be trapped in these open structures as well.

The position distribution is Gaussian as for the closed trap with a standard deviation of 0.60 μm (Figure 5b,c). The drift velocity is directed toward the trap center as well but contains a weak tangential component in the direction of the heating laser rotation (Figure 5d). This tangential contribution is due to the finite rotation speed of the heating laser. Especially close to the heated hole structure, drift velocity components appear that point radially away from the heated patch, as the laser is heating only one patch at a time. The particle is therefore pushed along the tangential direction. This component decreases with increasing rotation speed of the heating laser.

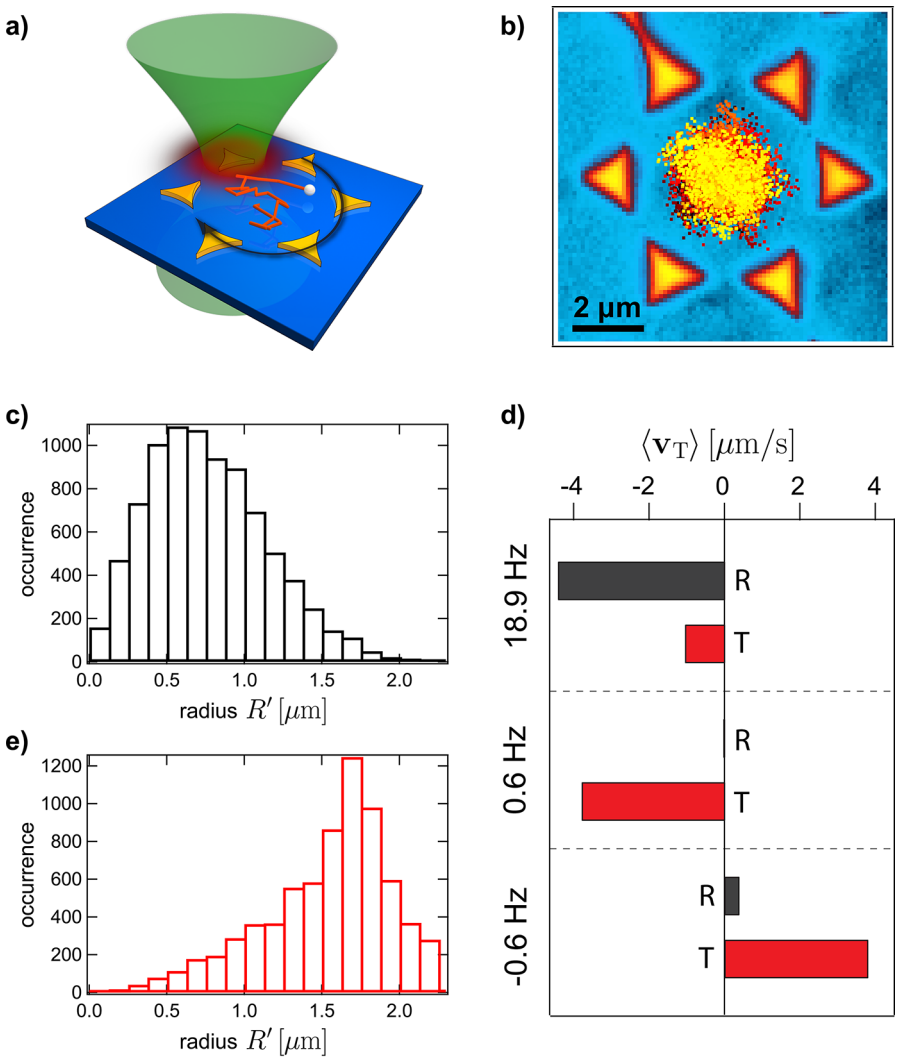

Figure 5. (a) Sketch of the focused heating beam illuminating only one gold pad of an open structure at a time. (b) Trajectory points of a 200 nm PS sphere trapped within an open gold structure at 5 mW heating power for a laser rotation frequency of 18.9 Hz (time color-coded, black to yellow). The wide-field laser illumination was kept at a power of 200 mW, only responsible for the fluorescence excitation of the colloidal particle. (c) Radial position distribution of the particle within the trap for 18.9 Hz. (d) Dependence of the radial (black) and tangential (red) thermophoretic drift on the laser rotation frequency. A positive frequency corresponds to a clockwise rotation, whereas a negative frequency indicates a counter-clockwise rotation of the laser beam. (e) Same as (c) but at a laser rotation frequency of 0.6 Hz.

Overall, the phenomenology observed for the patchy structure with a dynamic heating is the same as for the static heating scheme. Knowing the width of the particle distribution and the shape of the average temperature profile, we estimate an effective potential depth of about 11.8 k_BT from eqs 3 and 4 at an average temperature rise in the center of the trap of ΔT_{avg} = 9 K (see SI). As a result of the steeper temperature gradients in the patchy structure, a more effective trapping is achieved with lower heating powers. However, the main advantage of the dynamic heating scheme in combination with a large array of open gold structures (see Figure 1) is the scalability. A multitude of adjacent traps thus becomes possible where single particles or even single molecules can intentionally be released from one trap and arbitrarily guided over the sample by an appropriate heating. In combination with a dynamic heating even feedback schemes as employed for the ABEL trap are possible, which will further improve the trapping and manipulation efficiency in a single trap.

Beyond Trapping: Manipulating the Motion of PS Spheres. The appearance of a tangential drift velocity component as revealed in the previous paragraph demonstrates that even more complex manipulations of single nano-objects in a micrometer-sized trap are possible. In the simplest case, the position distribution of the particle may be modified in a way that the particle is occupying not only the center of the trap. For this purpose we decrease the angular velocity of the heating beam to 0.6 Hz, such that the velocity of the temperature field is comparable to the thermophoretic drift. As a consequence, the tangential drift velocity component increases and the radial component almost disappears. These results are depicted in

Figure 5d, where the average thermophoretic drift velocity components are shown for different heating laser rotation frequencies. While at high frequencies a radial drift velocity component dominates, it almost completely disappears for low frequencies, and a tangential drift velocity component determines the particle motion in the direction of heating laser rotation. Accordingly, the tangential velocity changes sign when changing the laser rotation direction.

The consequence of this missing radial drift velocity component is that the particle is not pushed to the center of the trap. Therefore, the particle is located at the rim of the trap, which becomes directly visible in the radial particle distribution (see Figure 5e). The particle now exhibits a circular motion within the trapping region (see movie in SI). This illustrates that single particles can be steered in a liquid by applying thermal gradients and paves the way for an all-optical controlled nanofluidic tool for the free manipulation of single or multiple particles where an adaptive heating will actively be controlled by a feedback on the particle's position.

CONCLUSION

We have demonstrated a new optically controlled method to trap and manipulate single nano-objects in solution. The method is based on the thermophoretic motion in temperature gradients and involves no body forces but only thermodynamic forces. Gold nanostructures are used as microscopic heat sources generating strong temperature gradients. The structures are shown to allow for a pure thermophoretic trapping of 200 nm particles in a stationary heating mode. A dynamic heating mode indicates the possibility to guide single particles through a liquid film by time-dependent artificial temperature landscapes that are controlled all-optically. The proposed technique can easily be integrated in lab-on-a-chip devices and extended to feedback-based trapping schemes, which may push the limits down to single molecules.

MATERIALS AND METHODS

Microsphere lithography is used to produce gold structures in large arrays on glass cover-slides.[29] By thermal evaporation a cover-slide is coated with a 5 nm chromium layer to enhance the adherence of the gold structure. Either single polystyrene spheres or a close-packed monolayer of PS spheres of 5.3 μm diameter is prepared on top of the cover-slide. After that gold is evaporated to form a layer of 50 nm thickness not only on top of the PS spheres but also within the region between the spheres, as can be seen in Figure 1a. The PS spheres are removed by ultrasonification, and remaining beads are dissolved in a toluene bath. Either single holes in the gold film or large-scaled hexagonal arrays of single gold islands (see Figure 1b) remain on the glass-slide depending on the preparation of the PS beads. The chromium film that is not covered by gold is removed by Chromium Etch No. 1 (MicroChemicals GmbH). For the experiments a second plain cover-slide is put on top to confine a water film containing dye-doped PS beads of 200 nm diameter. The height of the water film is adjusted to about 500 nm. Hence, the beads are not spatially confined to the trapping region but are able to diffuse between the gold film and the upper glass-slide. The trajectories of the beads are recorded by their fluorescence in an optical microscopy setup. It contains both a wide-field illumination ($\omega_{0,w} \approx 20$ μm) for fluorescence excitation as well as for heating the gold structure and a focused illumination of a second laser beam ($\omega_{0,f} \approx 1.0$ μm) for the heating of a single specific gold island. The focused beam can be steered laterally in the sample plane over an area of 50×50 μm^2 by an acusto-optic deflector (Brimrose). Both laser beams are of 532 nm wavelength. The fluorescence is collected by an Olympus objective lens (100×/NA1.3) and imaged to an Andor Ixon EMCCD camera using a tube lens of 50 cm focal length. Data were acquired at a frame rate of 100 Hz with a trajectory length of 500 s.

Conflict of Interest: The authors declare no competing financial interest.

Acknowledgment. This work was funded by the European Union and the Free State of Saxony. Financial support by the graduate school BuildMoNa and the Deutsche Forschungsgemeinschaft DFG (SFB TRR102) is acknowledged.

Supporting Information Available: A detailed description of the simulation of the temperature fields, a calculation of the temperature-dependent diffusion coefficient, the mean-squared displacement of a trapped particle, and the experimental setup. Three movies visualizing the different trapping modes. This material is available free of charge *via* the Internet at http://pubs.acs.org.

REFERENCES AND NOTES

1. Ashkin, A. Acceleration and Trapping of Particles by Radiation Pressure. *Phys. Rev. Lett.* **1970**, *24*, 156–159.
2. Grier, D. G. A Revolution in Optical Manipulation. *Nature* **2003**, *424*, 810–816.
3. Moffitt, J. R.; Chemla, Y. R.; Smith, S. B.; Bustamante, C. Recent Advances in Optical Tweezers. *Annu. Rev. Biochem.* **2008**, *77*, 205–228.
4. Juan, M. L.; Righini, M.; Quidant, R. Plasmon Nano-Optical Tweezers. *Nat. Photonics* **2011**, *5*, 349–356.
5. Juan, M. L.; Gordon, R.; Pang, Y.; Eftekhari, F.; Quidant, R. Self-Induced Back-Action Optical Trapping of Dielectric Nanoparticles. *Nat. Phys.* **2009**, *5*, 915–919.
6. Cohen, A. E.; Moerner, W. E. Method for Trapping and Manipulating Nanoscale Objects in Solution. *Appl. Phys. Lett.* **2005**, *86*, 093109.
7. Fields, A. P.; Cohen, A. E. Electrokinetic Trapping at the One Nanometer Limit. *Proc. Natl. Acad. Sci. U.S.A.* **2011**, *108*, 8937–8942.
8. Wang, Q.; Moerner, W. E. An Adaptive Anti-Brownian Electrokinetic Trap with Real-Time Information on Single-Molecule Diffusivity and Mobility. *ACS Nano* **2011**, *5*, 5792–5799.
9. Guan, W.; Joseph, S.; Park, J. H.; Krstić, P. S.; Reed, M. A. Paul Trapping of Charged Particles in Aqueous Solution. *Proc. Natl. Acad. Sci. U.S.A.* **2011**, *108*, 9326–9330.
10. Ludwig, C. Diffusion Zwischen Ungleich Erwärmten Orten Gleich Zusammen-Gesetzter Lösungen. *Sitzber. Kaiserl. Akad. Wiss. Math.-Natwiss. Kl.* **1856**, *20*, 539.
11. Braun, D.; Libchaber, A. Trapping of DNA by Thermophoretic Depletion and Convection. *Phys. Rev. Lett.* **2002**, *89*, 188103.
12. Duhr, S.; Braun, D. Two-Dimensional Colloidal Crystals Formed by Thermophoresis and Convection. *Appl. Phys. Lett.* **2005**, *86*, 131921.
13. Voit, A.; Krekhov, A.; Köhler, W. Laser-Induced Structures in a Polymer Blend in the Vicinity of the Phase Boundary. *Phys. Rev. E* **2007**, *76*, 011808.

14. Jiang, H.-R.; Wada, H.; Yoshinaga, N.; Sano, M. Manipulation of Colloids by a Nonequilibrium Depletion Force in a Temperature Gradient. *Phys. Rev. Lett.* **2009**, *102*, 208301.
15. Duhr, S.; Braun, D. Optothermal Molecule Trapping by Opposing Fluid Flow with Thermophoretic Drift. *Phys. Rev. Lett.* **2006**, *97*, 038103.
16. Duhr, S.; Braun, D. Why Molecules Move along a Temperature Gradient. *Proc. Natl. Acad. Sci. U.S.A.* **2006**, *103*, 19678–19682.
17. Weinert, F. M.; Braun, D. An Optical Conveyor for Molecules. *Nano Lett.* **2009**, *9*, 4264–4267.
18. Maeda, Y. T.; Tlusty, T.; Libchaber, A. Effects of Long DNA Folding and Small RNA Stem−Loop in Thermophoresis. *Proc. Natl. Acad. Sci. U.S.A.* **2012**, *109*, 17972–17977.
19. Piazza, R. Thermophoresis: Moving Particles with Thermal Gradients. *Soft Matter* **2008**, *4*, 1740–1744.
20. Würger, A. Thermal Non-Equilibrium Transport in Colloids. *Rep. Prog. Phys.* **2010**, *73*, 126601.
21. Piazza, R.; Parola, A. Thermophoresis in Colloidal Suspensions. *J. Phys.: Condens. Matter* **2008**, *20*, 153102.
22. Braibanti, M.; Vigolo, D.; Piazza, R. Does Thermophoretic Mobility Depend on Particle Size?. *Phys. Rev. Lett.* **2008**, *100*, 108303.
23. Duhr, S.; Braun, D. Thermophoretic Depletion Follows Boltzmann Distribution. *Phys. Rev. Lett.* **2006**, *96*, 168301.
24. Rohrbach, A. Stiffness of Optical Traps: Quantitative Agreement between Experiment and Electromagnetic Theory. *Phys. Rev. Lett.* **2005**, *95*, 168102.
25. Magde, D.; Webb, W. W.; Elson, E. L. Fluorescence Correlation Spectroscopy. III. Uniform Translation and Laminar Flow. *Biopolymers* **1978**, *17*, 361–376.
26. Rings, D.; Schachoff, R.; Selmke, M.; Cichos, F.; Kroy, K. Hot Brownian Motion. *Phys. Rev. Lett.* **2010**, *105*, 090604.
27. Benesch, T.; Yiacoumi, S.; Tsouris, C. Brownian Motion in Confinement. *Phys. Rev. E* **2003**, *68*, 021401.
28. Fayolle, S.; Bickel, T.; Würger, A. Thermophoresis of Charged Colloidal Particles. *Phys. Rev. E* **2008**, *77*, 041404.
29. Yang, S.-M.; Jang, S. G.; Choi, D.-G.; Kim, S.; Yu, H. K. Nanomachining by Colloidal Lithography. *Small* **2006**, *2*, 458–475.